Jian Yang ORCID iD: 0000-0002-7624-6045

Repurposing a bacterial prolidase for organophosphorus hydrolysis: reshaped catalytic cavity switches substrate selectivity

Jian Yang[a,c‡], Yun-Zhu Xiao[a,d‡], Ru Li[a,b], Yu Liu[a,b], Li-Juan Long[a,b,c*]

[a.] CAS Key Laboratory of Tropical Marine Bio-resources and Ecology, Guangdong Key Laboratory of Marine Materia Medica, South China Sea Institute of Oceanology, Chinese Academy of Sciences, Guangzhou 510301, People's Republic of China.

[b.] University of the Chinese Academy of Sciences, Beijing 100049, People's Republic of China.

[c.] Southern Marine Science and Engineering Guangdong Laboratory, Guangzhou 511458, People's Republic of China.

[d.] Shenzhen Key Laboratory of Microbial Genetic Engineering, College of Life Sciences and Oceanology, Shenzhen University, Shenzhen 518055, People's Republic of China.

[‡] These authors contribute equally to this work.

[*] Author for correspondence: Li-Juan Long, longlj@scsio.ac.cn

This article has been accepted for publication and undergone full peer review but has not been through the copyediting, typesetting, pagination and proofreading process, which may lead to differences between this version and the Version of Record. Please cite this article as doi: 10.1002/bit.27455.

Abstract

Enzyme promiscuity is critical to the acquisition of evolutionary plasticity in cells and can be recruited for high-value chemical synthesis or xenobiotic degradation. The molecular determinants of substrate ambiguity are essential to this activity; however, these details remain unknown. Here, we performed directed evolution of a prolidase to enhance its initially weak paraoxonase activity. The *in vitro* evolution led to an unexpected 1,000,000-fold switch in substrate selectivity, with a 30-fold increase in paraoxon hydrolysis and 40,000-fold decrease in peptide hydrolysis. Structural and *in silico* analyses revealed enlarged catalytic cavities and substrate repositioning as responsible for rapid catalytic transitions between distinct chemical reactions.

Graphic abstract

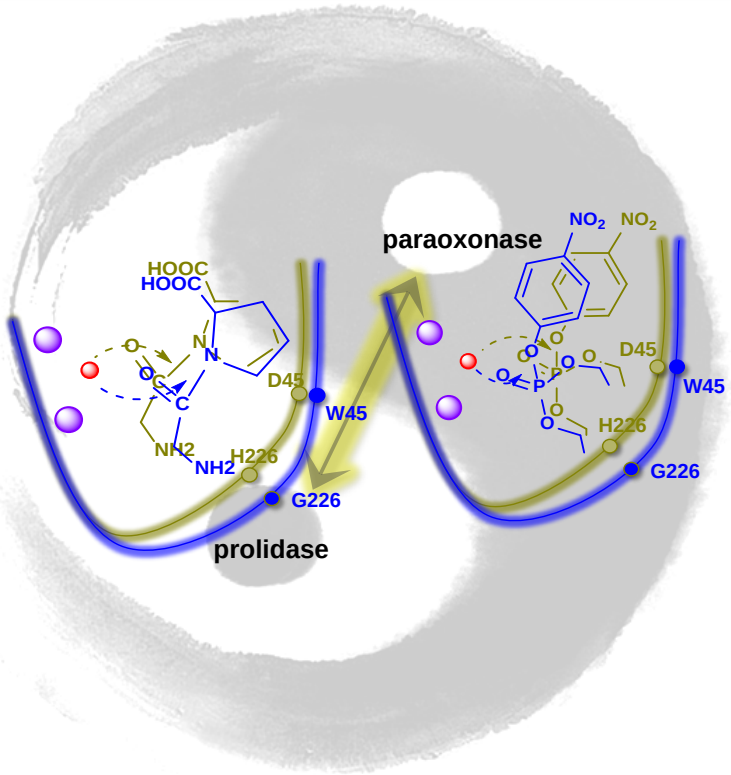

Keywords: enzyme promiscuity; active-site reshaping; protein engineering; substrate repositioning; catalytic selectivity

1. Introduction

The traditional view that enzymes are highly specific in their function has been profoundly revised by increasing observations that many enzymes are capable of catalyzing turnover of multiple substrates with substantially different molecular recognition properties (Pandya, Farelli, Dunaway-Mariano, & Allen, 2014; Toth-Petroczy & Tawfik, 2014). These promiscuous activities are assumed to provide evolutionary functionality that can be recruited and enhanced to facilitate organismal adaption to environmental changes, such as the emergence of antibiotics and anthropogenic chemicals (Brown, Schaab, Birmingham, & Armstrong, 2009; Copley, 2009). How enzymes satisfy the divergent and stringent requirements for multiple catalytic reactions is fascinating, but remains unclear. Elucidating the basis for enzyme promiscuity not only broadens the knowledge of enzyme evolution, but also provides invaluable insight into substrates recognition and catalysis that can be exploited to repurpose the enzyme reaction specificity (Nobeli, Favia, & Thornton, 2009). In the present study, we used a bacterial prolidase exhibiting promiscuous paraoxonase activity as a model system to understand the molecular origin of the substrate selectivity and promiscuity of the enzyme (Fig. 1a). In particular, we focused on regulating the catalytic pocket to repurpose the old scaffold enzyme with a new catalytic repertoire.

Prolidases are M24 peptidase family enzymes that exist in all species. Members of the M24 peptidase family constitute paradigmatic examples for studying how new functions emerge via the same protein fold.

The M24 peptidase family represents a large cluster of enzymes that catalyze a broad range of chemically distinct reactions, including peptide hydrolysis, creatine hydrolysis and demethylation (Xiao et al., 2017). In addition to exhibiting cross-wise catalytic activity, prolidases originating from bacteria (Cheng, Harvey, & Stroup, 1993; Stepankova et al., 2013; Xiao et al., 2017), archaea (Theriot, Du, Tove, & Grunden, 2010), and mammals (Wang, Zhi, & Sun, 2005) are capable of hydrolyzing phosphoester bonds in man-made phosphotriester substrates that were introduced into the environment only ~100 years ago. Structural studies of human and bacterial prolidases indicate shared active sites, with hydroxide bridging between two metal ions promoting nucleophilic attack on a phosphorus center or peptide bond (Daczkowski, Pegan, & Harvey, 2015; Wilk et al., 2017). Nevertheless, it remains unclear how prolidases recognize two distinct chemicals within the same active site, and whether *in vitro* evolution of preexisting active-site features can switch enzyme function.

Here, we attempt to identify the specificity determinants using the M24 peptidase family prolidase from *Pseudoalteromonas* sp. SCSIO 04301 as a model enzyme which exhibits promiscuous hydrolysis activity toward paraoxon with a k_{cat}/K_m value 100-fold lower relative to that of Gly-Pro (Xiao et al., 2017). We focus on the residues involving in substrate binding that are likely to cause a transition between activities of the enzyme. Laboratory evolution of the prolidase was performed to improve its paraoxon hydrolysis activity and structural and computational information of the evolved enzyme was analyzed. The resulting systematic analysis of the effects of residue substitutions on catalysis of different chemical reactions illustrates how reshaped substrate cavity alters substrate specificity, and addresses the molecular mechanisms associated with repurposing a promiscuous enzyme.

2. Materials and Methods

2.1 Protein purification

Wild-type and mutant proteins were expressed in *Escherichia coli* Rosseta (DE3) under the control of the T7 promoter as described previously (Xiao et al., 2017). Cells were lysed by sonication using 1 s pulse/ 1 s pause cycles. The cell debris was removed by centrifugation at 10,000 g for 30 min. The supernatant fraction was loaded onto an equilibrated Ni-NTA resin (QIAGEN). After extensively washing with wash buffer (10 mM Tris-HCl, pH8.0, 500 mM NaCl, 20 mM imidazole), the recombinant proteins were eluted with elution buffer (10 mM Tris-HCl, pH8.0, 500 mM NaCl, 200 mM imidazole). The eluate was further purified by loading onto a HiPrep DEAE FF column (GE Healthcare), and elution was performed with a linear gradient of 0-1.0 M NaCl. All purified proteins were concentrated with Vivaspin 20 devices (10,000 MWCO PED) (Storius).

2.2 Crystallization, X-ray diffraction, and structure determination

All crystallization trials were performed by hanging-drop vapor diffusion method. Crystals of OPAA4301 and D45W/H226G were obtained by mixing 0.4 μL of purified protein (10 mg/mL) with 0.4 μL of reservoir solution, and allowing the drop to equilibrate at 20 °C in 48-well protein crystalization plates. The reservoir solutions for crystallization of OPAA4301 and D45W/H226G were 100 mM MES (pH6.5), 5% (v/v) PEG400, and 2 M ammonium sulfate. A single protein crystal was picked up and soaked in the reservoir solution containing 20% (v/v) glycerol as a cryo-protectant, and a diffraction data set was collected on beamline SSRF-BL17U or SSRF-BL19U of National Center for Protein Science Shanghai

(China). The diffraction data were indexed, integrated, and scaled using XDS program (Kabsch, 2010). The crystal structure of 4ZWP was used as a model for molecular replacement by Phaser (McCoy et al., 2007). Iterative refinement cycles were performing using REFMACS (Murshudov et al., 2011), PHENIX (Adams et al., 2010), and COOT(Emsley & Cowtan, 2004). Data collection and refinement statistics are presented in Table S1. All structures were depicted by using PyMOL viewer (Version 2.3 Schrödinger, LLC).

2.3 Mutagenesis and screening

Primers were designed with the degenerate code "NNK" at target sites to generate mutants by one-step site-directed mutagenesis(Zheng, Baumann, & Reymond, 2004). The resultant linearized plasmid derivatives were transformed into *E. coli* XL1-Blue competent cells to obtain mutant plasmids; the saturation mutagenesis plasmid pools were then transformed into *E. coli* Rosetta (DE3) cells. Approximately 400 clones from each site-directed mutagenesis library were selected in 96-well plates containing 200 μl LB broth with 50 μg/ml of ampicillin and 0.2 mM IPTG. After culturing at 28°C for 48 h, cells were centrifuged at 4000 × *g* for 20 min at 4°C. The paraoxonase activity of each clone was compared to that of the wild type. Mutant enzymes with higher paraoxon-hydrolyzing ability were selected and the mutation was confirmed by DNA sequencing.

2.4 Enzyme assay

Paraoxonase activity was measured as previously described (Hiblot, Gotthard, Chabriere, & Elias, 2012) using paraoxon (Sigma-Aldrich, St. Louis, MO, USA) as substrate. The assay mixture containing 1 mM paraoxon, 0.05–0.5 μM enzyme, 200 μM $MnCl_2$, and 50 mM glycine-NaOH buffer (pH 8.5) was

incubated at 50°C for 30 min, and *p*-nitrophenol production was monitored with a spectrophotometer at 405 nm. One unit of paraoxonase activity was as defined as the amount of enzyme required to liberate 1.0 μmol *p*-nitrophenol per minute under standard conditions. Prolidase activity was determined with the Cd–ninhydrin method using Gly-Pro dipeptide as substrate (Doi, Shibata, & Matoba, 1981). The assay mixture contained 2 mM Gly-Pro, 0.05–1 μM purified enzyme, and 200 μM $MnCl_2$ in 50 mM borate buffer (pH 8.5). One unit of prolidase activity was defined as the amount of enzyme required to liberate 1.0 μmol glycine per minute at 50°C. For determination of kinetic parameters, a range of concentrations of paraoxon and dipeptide was prepared at final concentrations of 0.5–3.0 mM (0.5-mM interval) and 2–6 mM (1-mM interval), respectively.

2.5 Molecular dynamics (MD) simulation

The substrate-binding pocket for docking was identified based on atomic coordinates of human prolidase (PDB code no.: 5M4J) containing the substrate Gly-Pro bound to the manganese ion. The two ligands, paraoxon and dipeptide Gly-Pro, were docked to each of the receptor models at the putative active sites using the force field AMBER12:ETH. MD simulation was performed using AMBER14. Leap package of AMBER was used to add hydrogen atoms to each protein. Resulted models were then solvated in TIP3P water boxes with Ambertool. The systems were neutralized by adding counter ions (sodium or chlorine). Amber99SB force field was added for the protein and water box. The restrained electrostatic potential electric charges of ligands were calculated by Gaussian 09 and fitted with the program antechamber, and the Gaff force field was added for substrates. Each of the models was optimized in three steps: solvent optimization by constraining the coordinates of the whole protein and substrate; optimization of hydrogen

atoms of the protein backbone and substrate by constraining other heavy atoms; and final optimization by harmonic constraining of manganese ions. The entire system was equilibrated to 310 K over 10 ps, and pressure was equilibrated to 1 atm over 100 ps. Equilibrated conformations were used as the starting point of a 50-ns dynamic stimulation. A cutoff distance of 12 Å for van de Waals and electrostatic interactions was set for the stimulation process. Structures resulting from the 50-ns MD were used for QM/MM stimulations where manganese ions, substrates, residue Y212, H226, D244, D255, H336, R367, E381, E420, and D45 (chain B) were separated by the PM6 semi-empirical quantum chemical method. QM/MM stimulations ran for 20 ps.

3. Results and Discussion

3.1 Engineering of a prolidase for organophosphorus hydrolysis

We present the crystal structure of enzyme OPAA4301 at 2.6 Å resolution (Table S1) showing an overall structure of a homo-tetramer formed by dimer-of-dimers assembly with H32 symmetry (Fig. S1). The observed oligomeric state of the enzyme is consistent with previous results of gel filtration chromatography (Xiao et al., 2017), and each subunit possesses a highly conserved C-terminal pita-bread fold, where the two ions are separated at the bottom of the active cleft (Fig. 1b). Structural superposition of OPAA from *Alteromonas* sp. JD6.5 (Daczkowski et al., 2015; Vyas, Nickitenko, Rastogi, Shah, & Quiocho, 2010) and human prolidase (Wilk et al., 2017) indicated that the active site residues involved in ion coordination, substrate binding, or leaving-group stabilization are conserved in the concavity of the pita-bread fold (Figs. 1c and S2). Molecular docking of paraoxon (Fig. 1d) and Gly-Pro (Fig. 1e) as well as our previous results

of alanine scanning mutagenesis (Xiao et al., 2017) confirmed their roles in substrate binding. The catalytic power of enzymes is attributed to precisely organized active sites that stabilize transition states and lower activation energy (Kraut, Carroll, & Herschlag, 2003; Warshel, 2003), as well as extend networks of outer-shell interactions involved in catalysis by modulating sophisticated active site geometries or tuning Michaelis-complex binding patterns (Miton et al., 2018; Obexer et al., 2017). Hence, we hypothesized that the first-shell residues of the substrate pocket are hot spots for regulating promiscuous catalysis of paraoxon by enzyme OPAA4301.

Saturation mutagenesis (SM) libraries for the 11 conserved substrate binding residues were created and screened for improved paroaxonase activity. Repetitive variants were excluded by gene sequencing, and potential variants were confirmed by comparing the specific activities of purified mutant enzymes with wild-type (WT). A total of 16 hits with single point mutations were obtained from ~4,000 transformants. These mutations were located at five sites: the 226^{th} and 332^{th} residues, which are responsible for binding the large substituent of the native substrate (proline), the 45^{th} residue, which is responsible for binding of the small substituent (glycine), and the 292^{th} and 366^{th} residues, which are responsible for leaving group stabilization during catalysis (Fig. 1c and S3). Among these, the greatest increase in paraoxon hydrolysis (11.4-fold) was observed for the D45W mutant. Seven of the 16 variants were derived from the SM library of the 226^{th} residue and suggested that all but the charged amino acids in the active site were required for paraoxon hydrolysis. We subsequently selected five mutants showing the highest paraoxonase activity at each site (D45W, H226G, H332P, Y292F, and L366F) for combinatorial mutations. Two variants, H226G/H332P within the large binding group and Y292F/L366F within the leaving group, were generated,

resulting in decreased paraoxonase activity by H226G/H332P and a slight increase in activity (1.5-fold) by Y292F/L366F. We chose H226G in the large binding group, D45W in the small binding group, and Y292F/L366F in the leaving group for a further round of combinatorial mutagenesis between substrate-binding groups. Four more variants, including D45W/H226G, H226G/Y292F/L366F, D45W/Y292F/L366F, and D45W/H226G/Y292F/L366F, were generated and characterized, among which D45W/H226G exhibited the greatest (33.8-fold) improvement in specific activity over the WT enzyme (Fig. 2a).

3.2 Strong trade-off between native and promiscuous functions

To accurately quantify the effect of mutations on native and promiscuous activities, we determined and compared the kinetics parameters for both paraoxonase (promiscuous) and prolidase (native) activities of the purified variants. After three rounds of *in vitro* evolution of the substrate pocket of the bacterial prolidase, a final improvement of ~30-fold in promiscuous paraoxonase activity (k_{cat}/K_m=2.96×10^4 $M^{-1}\cdot s^{-1}$) was achieved. The evolved enzyme (D45W/H226G) shared the same K_m value with WT enzyme, with the enhanced catalytic efficiency (k_{cat}/K_m) for paraoxon mainly attributed to the increased k_{cat} value (Fig. 2b). The kinetic properties indicated that mutations at these sites influenced the catalytic process instead of altering the affinity of the enzyme for paraoxon. Interestingly, the mild prolidase activity of the enzyme was sensitive to mutations in the active sites. We detected obvious decreases in k_{cat}/K_m values for all of the selected mutations in the evolutionary trajectory (Table S2). Double mutations at the 45th and 226th sites caused the most significant reduction of 43,635-fold on Gly-Pro hydrolysis (k_{cat}/K_m=1.76 $M^{-1}\cdot s^{-1}$), which was due to the decrease in the k_{cat} value.

Evolutionary optimization of enzymes can reveal contradictory findings regarding multiple properties, such as widely addressed trade-offs concerning the stability and accuracy of catalytic activity (Elias, Wieczorek, Rosenne, & Tawfik, 2014; Tawfik, 2014). The results demonstrated a strong trade-off of native-promiscuous activity for acquisition of new function, as the mutant with strongly improved paraoxonase activity showed negligible prolidase activity. The differential effects of mutations resulting in a $>10^6$-fold change in substrate specificity confirmed the 45^{th} and 226^{th} residues as highly plastic "gatekeepers" that allow rapid specificity switching from prolidase to paraoxonase. These results are reminiscent of those obtained in arylsulfatase (Bayer, van Loo, & Hollfelder, 2017) and *N*-acetylneuraminic acid lyase (Campeotto et al., 2010), for which all of the substitutions at the target sites reduced their native activities and increased activities toward promiscuous substrates. Previous observations of directed evolution of entire enzyme-coding sequences (Khersonsky & Tawfik, 2010; Miton et al., 2018; Tokuriki et al., 2012) and systematic comparative study between promiscuous members in one superfamily (van Loo et al., 2019) revealed that primary function is robust to mutagenesis while promoting significant increases in new catalytic efficiency. The ability of mutational robustness can be a molecular solution to avoid adaptive conflict during evolution (Nasvall, Sun, Roth, & Andersson, 2012; Sikosek, Chan, & Bornberg-Bauer, 2012; van Loo et al., 2019). Yet, the results of present study reinforced that promiscuous reactions might be less affected by certain mutations relative to native activity, and the rapid transitions in activity and specificity observed in OPAA4301 demonstrated that the chemical function and specificity of an enzyme can be changed with only a few amino acid substitutions.

3.3 Expanded substrate specificity for organophosphirus

A series of 14 organophosphorus compounds with distinct chemical structures was tested as expanded substrates (Fig. 2c and d). All of the compounds are pesticides or flame retardants commercially used worldwide. We evaluated the specific activities of the WT OPAA4301 enzyme and D45W/H226G, with the WT enzyme showing a relatively narrow substrate specificity and undetectable catalytic activity for six of the compounds. The inactivity of the WT enzyme is likely due to the larger leaving-group structures of these compounds that cause steric hindrance. The D45W/H226G variant displayed expanded substrate specificity included all of the tested compounds as substrates. Among these variants, D45W/H226G exhibited 33.8-, 21.4-, and 23.2-fold higher hydrolytic activities for paraoxon, phoxim, and trizaophos, respectively. These results demonstrated that mutations at position 45 and 226 of OPAA4301 enabled the enzyme to accept complex organophosphorus compounds. Thermal-stability analysis of the enzymes provided hints regarding the underlying mechanisms for the broaden substrate specificity. Both the optimal temperature and T_{50}[15] values for D45W/H226G decreased (Fig. S4), indicating enhanced flexibility of the active sites. Moreover, structural plasticity of substrate-binding sites might facilitate the entry of larger compounds into the catalytic cleft to initiate the reaction.

3.4 D45W/H226G reshaped the active pocket of the enzyme

To investigate the molecular mechanisms responsible for alteration of catalytic specificity caused by the mutations, we solved the crystal structure of D45W/H226G under the same conditions as those for WT, and at a resolution of 2.38 Å. The backbone of the protein shares the same conformations between D45W/H226G and WT, with a root mean square deviation (RMSD) of 0.3 Å, and the position of bound metal ions and binding residues also remained unchanged. However, the active-site conformation appeared

altered by mutations of D45W and H226G (Fig. 3a and b). The D45W/H226G mutant possesses a larger active-site volume as compared with that of the WT enzyme (~4678 $Å^3$ vs. ~4582 $Å^3$), with the R-group of H226G and conformational changes in the 367^{th} and 45^{th} residues both responsible for enlarging the active-site cavity (Fig. 3c and d). The widened of active-site pocket satisfied the requirement for accommodating bulky substrates and was consistent with the observed broadening substrate specificity toward organophosphorus compounds by the D45W/H226G mutant.

3.5 Substrate repositioning associated with the switch from prolidase to paraoxonase

We then performed molecular dynamics (MD) simulations using the enzyme-substrate complexes of WT and D45W/H226G. The protein–ligand complexes were generated by molecular docking, with conventional 50-ns MD simulations first performed to stabilize each complex structure. The variation in RMSD of the backbones was equilibrated near 1.3 Å and 1.5 Å for the WT and D45W/H226G enzymes, respectively (Fig. S5). The higher backbone RMSD indicated greater flexibility of the protein, which was consistent with the experimentally observed reduction in thermal stability and extended substrate specificity induced by the mutations. It is also worth noting that the RMSDs acquired for the substrates during MD simulations agreed with their respective catalytic efficiencies (Fig. S6). The D45W/H226G mutant exhibited extremely low activity toward Gly-Pro, due to its ability to freely re-orientate within the trajectories with much higher RMSD values than those observed for the WT enzyme. By contrast, the catalytic activity of D45W/H226G increased on paraoxon, which remained more stable in the active site, which showed a lower RMSD value than that of the WT enzyme.

We then performed a 20-ps quantum mechanics/molecular mechanics (QM/MM) simulation based on the proposed catalytic mechanisms (Fig. S7) to understand the origin of evolved substrate selectivity. As corroborated by QM/MM simulations, the switch between promiscuous and native reactions can be ascribed to the repositioning of substrate states with respect to the active sites. In the case of paraoxon hydrolysis, the hydrogen-bond interaction between residues D45 and R367 in the WT enzyme was lost due to the D45W mutation, which also introduced steric hindrance with residue R367 (Fig. 4a). Additionally, the R367 side chain displayed an altered conformation that tended to attract the nitryl group of paraoxon via a hydrogen bond. Moreover, the disappearance of the π-π-stacking effect between the imidazole group of the histidine and the nitro-phenol ring of paraoxon following H226G substitution contributed to the repositioning of paraoxon. Therefore, the in-line positioning of WT between hydroxide and phosphorus centers was optimized by evolution (angle OH^--P-O_{LG} ~160° in WT vs. ~164° in D45W/H226G). Moreover, the substrate paraoxon is comparatively shifted by 0.23-Å closer to the OH^- attacking phosphotriester bond (OH^--P, from 3.07 to 2.84 Å), which was 0.14-Å closer to the manganese ion (MnA-O_P, from 2.33 to 2.19 Å) (Fig. 4b). Shortened distances between substrate and key active-site residues can facilitate the formation of efficient Michaelis complexes with paraoxon for enhanced catalysis. In the case of Gly-Pro hydrolysis, the D45W and H226G mutations weakened interactions between Gly-Pro and the enzyme. For the WT enzyme, the carboxyl group of Gly-Pro interacts with R367 and H226 by hydrogen bonding, with this interaction absent from D45W/H226G (Fig. 4c). Additionally, the distances of both active OH^- groups to the carbon atom of the peptide bond (from 2.76 to 2.91 Å) and the MnA ion to the oxygen atom of the peptide bond (from 2.19 to 2.28 Å) increased in the D45W/H226G mutant (Fig. 4d).

The origins of enzyme promiscuity and the underlying mechanisms associated with how new catalysis evolves have garnered increased attention due to their theoretical and practical importance. The theory of conformational diversity of enzymes was proposed as a facilitator of catalytic promiscuity (Henzler-Wildman & Kern, 2007; Honaker, Acchione, Sumida, & Atkins, 2011), and directed evolution can enrich the small fraction of conformers interacting with promiscuous substrates to generate new conformational equilibria (Campbell et al., 2016; Ma & Nussinov, 2016). Contrary to expectations, we did not observe obvious shifts in equilibrium *via* dynamic conformational populations between the WT and D45W/H226G enzymes by principal component analysis. Nevertheless, we found that substrate positioning caused by the reshaped active site was responsible for the catalytic selectivity of enzymes. Our finding was consistent with that of another study applying directed evolution of sulfatase for phosphonate hydrolysis leading to an efficient charge offset in transition state (Miton et al., 2018). The distances and reaction angles of the substrates to facilitate formation of the nucleophile hydroxide correlated with catalytic efficiency, thereby providing evidence of the formation of new enzyme-substrate complexes supporting increases in catalytic efficiency.

4. Conclusion

In summary, we performed laboratory evolution of a bacterial prolidase to acquire enhanced promiscuous paraoxonase activity, and revealed a “strong negative trade-off” pattern in the acquisition of new catalytic activity. The evolved enzyme possessed a specificity switch of $>10^6$-fold, with a 30-fold increase in promiscuous activity and a 40,000-fold decrease in native activity. Additionally, the D45W/H226G mutant exhibited expanded substrate specificity toward organophosphorus compounds.

Based on analyses of the crystal structural and QM/MM simulations, we proposed that the reshaped active site can perturb substrate positioning to facilitate rapid transition between native and promiscuous catalysis. This study promotes understanding of molecular determinants of enzyme promiscuity and catalytic selectivity.

Acknowledgement

This work was supported by the "Strategic Priority Research Program" of the Chinese Academy of Sciences (XDA13020301); Science and Technology Project of Guangzhou (201904010165); Guangdong Natural Science Foundation (2019A1515011629); Key Special Project for Introduced Talents Team of Southern Marine Science and Engineering Guangdong Laboratory (Guangzhou) (GML2019ZD0402), National Natural Science Foundation of China (41406193); and Administration of Ocean and Fisheries of Guangdong Province (GD2012-D01-002). We thank Professor Changsheng Zhang (South China Sea Institue of Oceanology, CAS) for advice, Liping Zhang (South China Sea Institue of Oceanology, CAS) and Yuqun Xu (Southern University of Science and Technology) for crystallographic support.

References

Adams, P. D., Afonine, P. V., Bunkoczi, G., Chen, V. B., Davis, I. W., Echols, N.,... Zwart, P. H. (2010). PHENIX: a comprehensive Python-based system for macromolecular structure solution. *Acta Crystallographica. Section D: Biological Crystallography, 66*(2), 213-221. doi:10.1107/S0907444909052925

Bayer, C. D., van Loo, B., & Hollfelder, F. (2017). Specificity effects of amino acid substitutions in promiscuous hydrolases: context-dependence of catalytic residue contributions to local fitness landscapes in nearby sequence space. *ChemBioChem, 18*(11), 1001-1015. doi:10.1002/cbic.201600657

Brown, D. W., Schaab, M. R., Birmingham, W. R., & Armstrong, R. N. (2009). Evolution of the antibiotic resistance protein, FosA, is linked to a catalytically promiscuous progenitor. *Biochemistry, 48*(9), 1847-1849. doi:10.1021/bi900078q

Campbell, E., Kaltenbach, M., Correy, G. J., Carr, P. D., Porebski, B. T., Livingstone, E. K.,... Jackson, C. J. (2016). The role of protein dynamics in the evolution of new enzyme function. *Nature Chemical Biology, 12*(11), 944-950. doi:10.1038/nchembio.2175

Campeotto, I., Bolt, A. H., Harman, T. A., Dennis, C., Trinh, C. H., Phillips, S. E. V.,... Berry, A. (2010). Structural insights into substrate specificity in variants of N-acetylneuraminic acid lyase produced by directed evolution. *Journal of Molecular Biology, 404*(1), 56-69. doi:10.1016/j.jmb.2010.08.008

Cheng, T. C., Harvey, S. P., & Stroup, A. N. (1993). Purification and properties of a highly active organophosphorus acid anhydrolase from *Alteromonas undina*. *Appllied and Environmental Microbiology, 59*(9), 3138-3140. doi: 10.1128/AEM.59.9.3138-3140.1993

Copley, S. D. (2009). Evolution of efficient pathways for degradation of anthropogenic chemicals. *Nature Chemical Biology, 5*(8), 559-566. doi:10.1038/nchembio.197

Daczkowski, C. M., Pegan, S. D., & Harvey, S. P. (2015). Engineering the organophosphorus acid anhydrolase enzyme for increased catalytic efficiency and broadened stereospecificity on Russian VX. *Biochemistry, 54*(41), 6423-6433. doi:10.1021/acs.biochem.5b00624

Doi, E., Shibata, D., & Matoba, T. (1981). Modified colorimetric ninhydrin methods for peptidase assay. *Analytical Biochemistry, 118*(1), 173-184. doi: 10.1016/0003-2697(81)90175-5

Elias, M., Wieczorek, G., Rosenne, S., & Tawfik, D. S. (2014). The universality of enzymatic rate-temperature dependency. *Trends in Biochemical Sciences, 39*(1), 1-7. doi:DOI 10.1016/j.tibs.2013.11.001

Emsley, P., & Cowtan, K. (2004). Coot: model-building tools for molecular graphics. *Acta Crystallographica. Section D: Biological Crystallography, 60*(12), 2126-2132. doi:10.1107/S0907444904019158

Henzler-Wildman, K., & Kern, D. (2007). Dynamic personalities of proteins. *Nature, 450*(7172), 964-972. doi:10.1038/nature06522

Hiblot, J., Gotthard, G., Chabriere, E., & Elias, M. (2012). Characterisation of the organophosphate hydrolase catalytic activity of SsoPox. *Scientific Reports, 2*, 779. doi:10.1038/srep00779

Honaker, M. T., Acchione, M., Sumida, J. P., & Atkins, W. M. (2011). Ensemble perspective for catalytic promiscuity: calorimetric analysis of the active site conformational landscape of a detoxification enzyme. *Journal of Biological Chemistry, 286*(49), 42770-42776. doi:10.1074/jbc.M111.304386

Kabsch, W. (2010). Integration, scaling, space-group assignment and post-refinement. *Acta Crystallographica. Section D: Biological Crystallography, 66*(2), 133-144. doi:10.1107/S0907444909047374

Khersonsky, O., & Tawfik, D. S. (2010). Enzyme promiscuity: a mechanistic and evolutionary perspective. *Annual Review of Biochemistry, 79*, 471-505. doi:10.1146/annurev-biochem-030409-143718

Kraut, D. A., Carroll, K. S., & Herschlag, D. (2003). Challenges in enzyme mechanism and energetics. *Annual Review of Biochemistry, 72*, 517-571. doi:10.1146/annurev.biochem.72.121801.161617

Ma, B., & Nussinov, R. (2016). Protein dynamics: Conformational footprints. *Nature Chemical Biology, 12*(11), 890-891. doi:10.1038/nchembio.2212

McCoy, A. J., Grosse-Kunstleve, R. W., Adams, P. D., Winn, M. D., Storoni, L. C., & Read, R. J. (2007). Phaser crystallographic software. *Journal of Appllied Crystallography, 40*(4), 658-674. doi:10.1107/S0021889807021206

Miton, C. M., Jonas, S., Fischer, G., Duarte, F., Mohamed, M. F., van Loo, B.,... Hollfelder, F. (2018). Evolutionary repurposing of a sulfatase: A new Michaelis complex leads to efficient transition state charge offset. *Proceedings of the Nnational Academy of Sciences of the United States of America, 115*(31), 7293-7302. doi:10.1073/pnas.1607817115

Murshudov, G. N., Skubak, P., Lebedev, A. A., Pannu, N. S., Steiner, R. A., Nicholls, R. A.,... Vagin, A. A. (2011). REFMAC5 for the refinement of macromolecular crystal structures. *Acta*

Crystallographica. Section D: Biological Crystallography, 67(4), 355-367. doi:10.1107/S0907444911001314

Nasvall, J., Sun, L., Roth, J. R., & Andersson, D. I. (2012). Real-time evolution of new genes by innovation, amplification, and divergence. *Science, 338*(6105), 384-387. doi:10.1126/science.1226521

Nobeli, I., Favia, A. D., & Thornton, J. M. (2009). Protein promiscuity and its implications for biotechnology. *Nature Biotechnology, 27*(2), 157-167. doi:10.1038/nbt1519

Obexer, R., Godina, A., Garrabou, X., Mittl, P. R., Baker, D., Griffiths, A. D., & Hilvert, D. (2017). Emergence of a catalytic tetrad during evolution of a highly active artificial aldolase. *Nature Chemistry, 9*(1), 50-56. doi:10.1038/nchem.2596

Pandya, C., Farelli, J. D., Dunaway-Mariano, D., & Allen, K. N. (2014). Enzyme Promiscuity: Engine of Evolutionary Innovation. *Journal of Biological Chemistry, 289*(44), 30229-30236. doi:10.1074/jbc.R114.572990

Sikosek, T., Chan, H. S., & Bornberg-Bauer, E. (2012). Escape from Adaptive Conflict follows from weak functional trade-offs and mutational robustness. *Proceedings of the Nnational Academy of Sciences of the United States of America, 109*(37), 14888-14893. doi:10.1073/pnas.1115620109

Stepankova, A., Duskova, J., Skalova, T., Hasek, J., Koval', T., Ostergaard, L. H., & Dohnalek, J. (2013). Organophosphorus acid anhydrolase from Alteromonas macleodii: structural study and functional

relationship to prolidases. *Acta Crystallographica Section F-Structural Biology and Crystallization Communications, 69*, 346-354. doi:Doi 10.1107/S1744309113002674

Tawfik, D. S. (2014). Accuracy-rate tradeoffs: how do enzymes meet demands of selectivity and catalytic efficiency? *Current Opinion in Chemical Biology, 21*, 73-80. doi:10.1016/j.cbpa.2014.05.008

Theriot, C. M., Du, X. L., Tove, S. R., & Grunden, A. M. (2010). Improving the catalytic activity of hyperthermophilic *Pyrococcus* prolidases for detoxification of organophosphorus nerve agents over a broad range of temperatures. *Applied Microbiology and Biotechnology, 87*(5), 1715-1726. doi: 10.1007/s00253-010-2614-3

Tokuriki, N., Jackson, C. J., Afriat-Jurnou, L., Wyganowski, K. T., Tang, R., & Tawfik, D. S. (2012). Diminishing returns and tradeoffs constrain the laboratory optimization of an enzyme. *Nature Communications, 3*, 1257. doi:10.1038/ncomms2246

Toth-Petroczy, A., & Tawfik, D. S. (2014). The robustness and innovability of protein folds. *Current Opinion in Structural Biology, 26*, 131-138. doi:10.1016/j.sbi.2014.06.007

van Loo, B., Bayer, C. D., Fischer, G., Jonas, S., Valkov, E., Mohamed, M. F.,... Hollfelder, F. (2019). Balancing specificity and promiscuity in enzyme evolution: multidimensional activity transitions in the alkaline phosphatase superfamily. *Journal of the American Chemical Society, 141*(1), 370-387. doi:10.1021/jacs.8b10290

Vyas, N. K., Nickitenko, A., Rastogi, V. K., Shah, S. S., & Quiocho, F. A. (2010). Structural insights into the dual activities of the nerve agent degrading organophosphate anhydrolase/prolidase. *Biochemistry, 49*(3), 547-559. doi:10.1021/bi9011989

Wang, S. H., Zhi, Q. W., & Sun, M. J. (2005). Purification and characterization of recombinant human liver prolidase expressed in Saccharomyces cerevisiae. *Archives of Toxicology, 79*(5), 253-259. doi:10.1007/s00204-004-0634-4

Warshel, A. (2003). Computer simulations of enzyme catalysis: methods, progress, and insights. *Annual Review of Biophysics and Biomolecular Structure, 32*, 425-443. doi:10.1146/annurev.biophys.32.110601.141807

Wilk, P., Uehlein, M., Kalms, J., Dobbek, H., Mueller, U., & Weiss, M. S. (2017). Substrate specificity and reaction mechanism of human prolidase. *FEBS Journal, 284*(17), 2870-2885. doi:10.1111/febs.14158

Xiao, Y. Z., Yang, J., Tian, X. P., Wang, X. X., Li, J., Zhang, S., & Long, L. J. (2017). Biochemical basis for hydrolysis of organophosphorus by a marine bacterial prolidase. *Process Biochemistry, 52*, 141-148. doi:10.1016/j.procbio.2016.10.008

Zheng, L., Baumann, U., & Reymond, J. L. (2004). An efficient one-step site-directed and site-saturation mutagenesis protocol. *Nucleic Acids Research, 32*(14), e115. doi:10.1093/nar/gnh110

Figures

Figure 1. Structure of marine bacterial prolidase OPAA4301 and residue arrangements of the putative substrate pocket. (a) The hydrolysis of paraoxon and Gly-Pro catalyzed by OPAA4301, indicating promiscuous paraoxonase activity of via the prolidase fold. (b) Ribbon representation of the overall OPAA4301 structure. N- and C-terminal domains are indicated in yellow and green colors, respectively. (c) Superposed structures of OPAA4301 (PDB code no.: 6AH8, green), OPAA from *Alteromonas* sp. AJ6.5 (PDB code no.: 4ZWO, orange), and prolidase form human (PDB code no.: 5M4J, white). Proposed binding mode of paraoxon (d) and Gly-Pro (e) in the substrate pocket of OPAA4301.

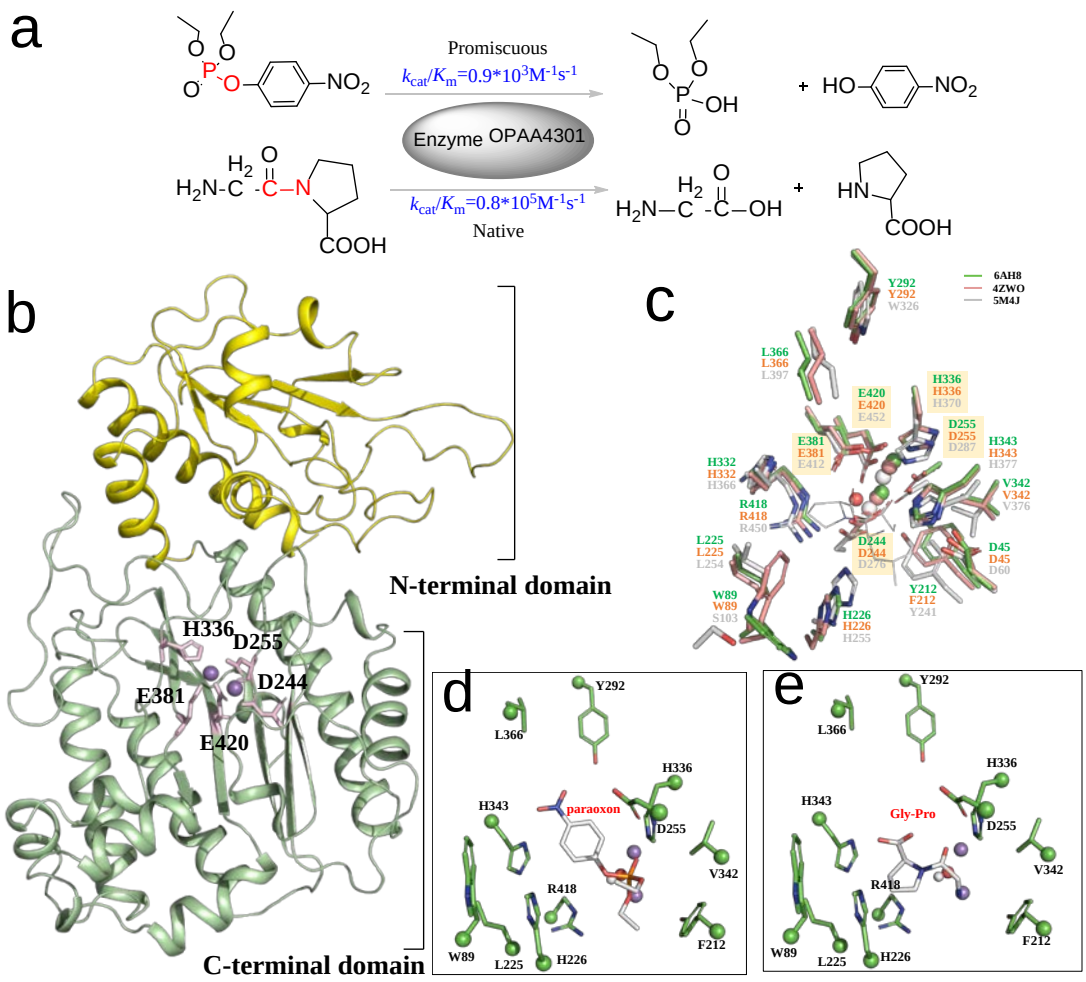

Figure 2. Evolution of prolidase OPAA4301 for organophosphorus hydrolysis. (a) Three rounds of directed evolution of the OPAA4301 active site to enhance paraoxonase activity. (b) Kinetic parameters for WT and D45W/H226G for paraoxon and Gly-Pro. (c) The D45W/H226G mutant exhibited broad substrate specificity for organophosphorus compounds. (d) Chemical structures of organophosphorus compounds tested for determination of substrate specificity.

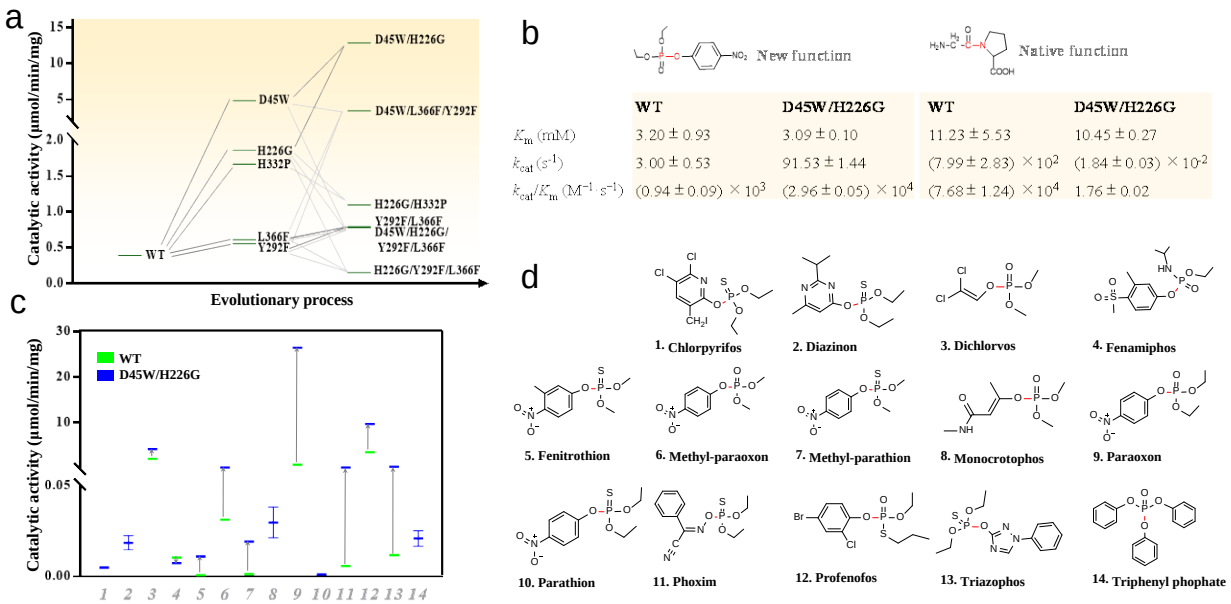

Figure 3. Reshaping of the active site pocket by directed evolution. Cavity volumes of the WT (a) and D45W/H226G (b) enzymes were calculated using POCASA server (http://altair.sci.hokudai.ac.jp/g6/service/pocasa/). Active-site representations of (c) WT (PDB ID: 6AH8) and (d) D45W/H226G (PDB ID: 6AH7) highlighting evolutionary reshaping.

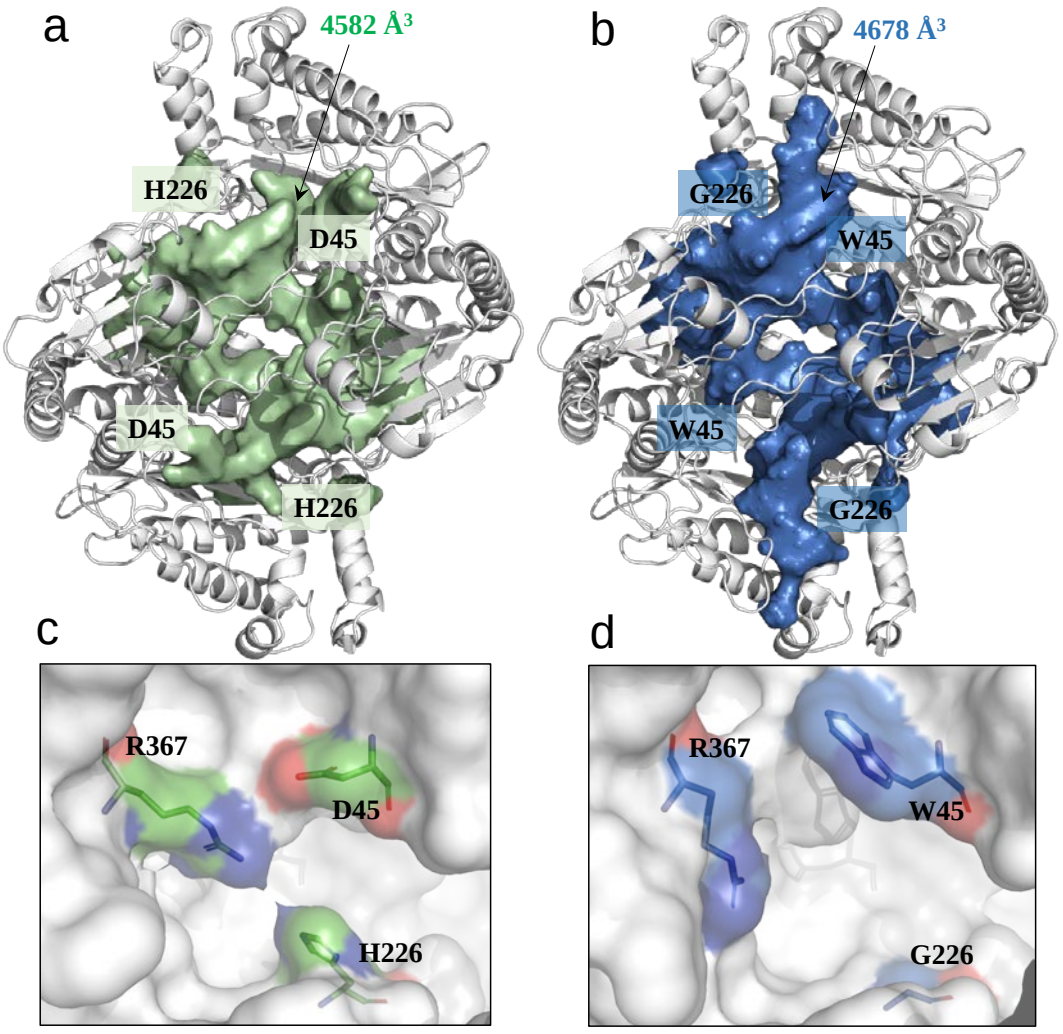

Figure 4. Substrate repositioning induced by the D45W and H226G mutation in OPAA4301. Representative stationary points from QM/MM simulation for (a) paraoxon and (b) Gly-Pro binding by the WT and D45W/H226G enzymes. Evolution of averaged distances and angle between key residues and (c) paraoxon or Gly-Pro for metal coordination and nucleophilic attack.